Materials Advances

PAPER

Check for updates

Tuning triboelectric and energy harvesting properties of dielectric elastomers *via* dynamic ionic crosslinks†

Xiao Hu, [ab] Runan Zhang,[c] Alan M. Wemyss, [b] Mohamed A. Elbanna, [d] Ellen L. Heeley, [e] Mustafa Arafa,[d] Chris Bowen, [c] Shifeng Wang,[f] Xueyu Geng*[b] and Chaoying Wan *[a]

The bromination of poly(isobutylene-*co*-isoprene) rubber introduces a small amount of bromide groups (1–2 mol%) to the elastomer backbone and creates new opportunities for functionalisation, as compared to other saturated and diene elastomers. In this work, three types of nucleophile reagents: namely pyridine, triphenylphosphine and imidazoles bearing four types of side groups of methyl, ethyl, hydroxyl or vinyl group were introduced to brominated poly(isobutylene-*co*-isoprene) rubber (BIIR) through nucleophile substitution with the bromine *via* solid-state rubber compounding and curing processes. The resulted ionic aggregates act as physical crosslinks and their size and density directly affected the mechanical reinforcement, self-healing and dynamic mechanical properties of the elastomers. The smaller and polar imidazolyl/bromine pairs led to the highest reinforcement beyond even the sulfur-cured BIIR counterparts. The 1-ethyl imidazole (EIm) modified BIIR showed the highest tensile strength of 17.01 ± 1.89 MPa and elongation at break of 1402 ± 69% with self-healing efficiency of 63.7%, after being treated at 140 °C for 30 min. In addition, the inclusion of the ionic clusters enhanced the relative permittivity of the elastomer, thereby enhancing the energy conversion efficiencies. The nucleophile substitution reaction *via* conventional solid-state rubber compounding processes provides a facile crosslinking and reinforcement strategy for halogen-containing polymers. In addition, the dynamic ionic crosslinking networks spontaneously benefit electromechanical and self-healing properties of the dielectric elastomers.

1. Introduction

The bromination of poly(isobutylene-*co*-isoprene) (IIR) provides the butyl elastomer with unique properties, including enhanced air-impermeability, high adhesion, high levels of antioxidation and good compatibility with other unsaturated elastomers. The small amount (1–2.0 mol%) of allylic bromide group is reactive to nucleophilic substitution with tertiary amines, imidazoles, or pyridines, which introduces pendant ionic groups along the polymer backbone and forms a macromolecular 'ionic liquid'-type elastomer.[1] The ionic groups interact and aggregate into ionic clusters that act as physical crosslinks for the elastomers, which can potentially lead to enhanced mechanical strength, flexibility, damping and self-healing properties, due to the dynamic and reversible-exchange nature of the ionic interactions.[1,2]

Parent and coworkers have investigated the synthesis and characterisation of IIR based ionomers in detail.[1,3–11] The solution-borne IIR derivatives bearing reactive functionalities, such as carboxyl group, ester group and ether group, were prepared by nucleophile substitution of BIIR.[3,11,12] With respect to pyridine or imidazole nucleophile substitution of BIIR, the structure and chain length of the nucleophiles, and the substitution sited on the heterocyclic ring affect the structure and properties of the ionic clusters, which subsequently influence the mechanical properties and self-healing efficiency of the ionic-modified elastomers.[13,14] Previous studies have shown that the introduction of pyridine derivatives tethered with –H, –CH$_3$ and –C(CH$_3$)$_3$ onto the fourth carbon of the pyridine ring increases the interaction between pyridyl cations

a International Institute for Nanocomposites Manufacturing (IINM), WMG, University of Warwick, CV4 7AL, UK. E-mail: chaoying.wan@warwick.ac.uk

b School of Engineering, University of Warwick, CV4 7AL, UK. E-mail: xueyu.geng@warwick.ac.uk

c Department of Mechanical Engineering, University of Bath, BA2 7AY, UK

d Department of Mechanical Engineering, American University in Cairo, New Cairo 11835, Egypt

e School of Life, Health and Chemical Sciences, The Open University, MK7 6AA, UK

f School of Chemistry and Chemical Engineering, Shanghai Jiao Tong University, 200240, China

† Electronic supplementary information (ESI) available. See DOI: https://doi.org/10.1039/d2ma00124a

and bromine anions and gives rise to a conversion ratio in excess of 70% due to the electron-donating effect. This becomes prominent in the case of a larger substituent size, thus the BIIR ionomer derived from –C(CH$_3$)$_3$ tethered pyridine exhibited high mechanical strength of 8.1 ± 0.3 MPa.[15]

By comparing 1-alkyl imidazole of various substituents including methyl, butyl, hexyl, nonyl, and 1-(6-chlorohexyl), the ionic-modified BIIR containing methyl substituent of the imidazole demonstrated the highest tensile strength 16.9 ± 2.9 MPa and a high elongation at break of 980 ± 30%, however, the material exhibited a low self-healing efficiency. In contrast, longer alkyl substituents led to a lower strength and larger elongation, but higher self-healing efficiency. The shorter substituents may form denser ionic clusters with stronger ionic interactions, thereby reducing the mobility of the ionic groups and improving mechanical reinforcement; while the longer alkyl substituents tend to have weaker ionic interactions thereby improving the self-healing efficiency.[13] Optimised mechanical and self-healing properties were found in the BIIR ionomer containing imidazolium moiety bearing hexyl substituent, showing up to 74% of healing efficiency with regard to tensile strength and 98% healing efficiency for the elongation at break after healing at 70 °C for 16 h.[13] Therefore, the mechanical and self-healing properties of BIIR ionomers can be tuned by the size and strength of the ionic clusters. The size, strength and reactivity of the ionic clusters formed as a result of the alkylation reactions between BIIR elastomers and nucleophiles are highly dependent on the chemical structure, side-chain length and substitution ratios.[13,14]

Current soft energy harvesting devices have been dominated by hydrogels, silicone rubbers and acrylic rubbers, which have inherent limitations, such as permanently crosslinked structures, low dielectric constant (relative permittivity) and high viscoelastic loss. The reversible exchangeable ionic bonds offer unique approaches towards reinforcement with high extensibility, and their electropositivity may provide a route to increase the polarity and dielectric permittivity of elastomers. The enhancement of both the mechanical and dielectric properties provide new opportunities for the elastomeric ionomers in actuation and energy harvesting applications. In particular, the polarity and dielectric permittivity of the elastomers can be designed and tuned by varying the size and density of the ionic crosslinks. Here the effects of the size and structure of different alkylation nucleophiles on the mechanical, self-healing, polarity and electromechanical properties of BIIR ionomers are investigated. The performance of the dielectric BIIR ionomers is further demonstrated in triboelectric, actuation and energy harvesting applications. The ionic structure–dielectric properties relationships of the elastomer ionomers are discussed.

2. Experimental

2.1 Materials

BIIR (X-Butyl B2030), with the bromide content of 1.523 mol%, was provided by Arlanxeo Co., Ltd; Chemicals, 1-ethyl imidazole (EIm, 97%) 1,2-dimethyl imidazole (DMIm, 97%), 1-(2-hydroxyethyl)imidazole (HEIm, 97%), 1-vinyl imidazole (VIm, 97%), pyridine (PD, ≥99%) and triphenylphosphine (PPh$_3$, 99%) were purchased from Sigma-Aldrich, UK. All chemicals were used as received.

2.2 Ionic modification of BIIR *via* alkylation nucleophile substitution through a solid-state process

BIIR (45 g, 6.75 mmol allylic bromide) was compounded with a range of *N*-substituted imidazoles, including 1-ethyl imidazole (EIm), 1,2-dimethyl imidazole (DMIm), 1-(2-hydroxyethyl) imidazole (HEIm), 1-vinyl imidazole (VIm), pyridine (PD) or triphenylphosphine (PPh$_3$), using a HAAKE Polylab internal mixer at 40 °C with a rotation speed of 60 rpm for 15 min. The amount of alkyl imidazoles and PD were 1.65 equivalent to bromide content of BIIR in mole to ensure a high conversion,[13] and the amount of PPh$_3$ was 1.2–1.6 equivalent bromide content were investigated. The mixtures were further compression-moulded into elastomer sheets at 140 °C for 30 min under 12 MPa.

2.3 Characterisation

Curing properties of the elastomers were evaluated using MDR 3000 Rheometer at 140 °C in standard mode with an angle of 0.50° and a frequency of 1.67 Hz. 2D Small-Angle X-ray Scattering (SAXS) data for all samples was collected using a Xenocs Xeuss 2.0 instrument with a Cu K$_\alpha$ source (λ = 1.54 Å). The 2D SAXS data was collected on a Pilatus 300K detector, where an evacuated chamber of 1.2 m was situated between the sample and detector reducing air scattering and absorption. All measurements were made at 25 °C. Thin film samples of 200 μm were attached to a vertical sample holder in an evacuated sample chamber. For each sample the SAXS data collection time was 10 minutes. The SAXS detector was calibrated with silver behenate. All data were normalized for sample thickness, transmission and background scattering using the Xeuss 2.0 analysis software. Further data reduction was performed on the 2D SAXS patterns where 1D scattering profiles of intensity I, *versus* scattering vector q, (where $q = (4\pi/\lambda)\sin(\theta)$, 2θ is the scattering angle and λ is the X-ray wavelength) were obtained by sector averaging around the beam stop by a fixed angle and radius, q.

FTIR spectra were collected from a Bruker TENSOR 27 with a resolution of 4 cm^{-1} and 32 scans in transmission mode. To remove the influence of the residue of nucleophiles on the spectra, all samples were soaked in toluene for 72 h and then dried in vacuum for 96 h before testing. For the temperature-dependent FTIR measurement, an additional Specac Eurotherm 2216e heating stage was attached, the samples were scanned with 10 °C increase intervals from 30 to 140 °C. The samples were allowed to equilibrate at each temperature for 10 min before measurement.

Before the ^{1}H NMR measurement, samples were purified by precipitating in methanol after being dissolved in THF anhydrous solution containing a few drops of acetic acid. The samples were dried in a vacuum oven at 50 °C for 72 h to a constant weight. For insoluble samples, the swelled region was removed, and the dissolved part was purified through the above steps. After two-times precipitation, the purified remains were

dissolved in chloroform-D. The ^{1}H NMR spectra were recorded using a Bruker Avance III HD 300 MHz spectrometer. Chemical shifts were internally referenced to TMS using CDCl$_3$. Spectra were processed using ACD/NMR processor version 12.01.

Dynamic mechanical thermal analysis (DMTA) of the samples was conducted using a Triton Tritec 2000 DMA in tension mode with a static strain of 0.05 and frequency of 10 Hz. The heating rate was 3 K min^{-1} from −80 to 150 °C. The sample sizes used were 5.0 mm × 10.0 mm × 1.0 mm.

Tensile tests were conducted using a Shimadzu Autograph AGS-X with the speed of 500 mm min^{-1} at room temperature according to ASTM-D638-14 type V. Cyclic stress softening tests were performed by extending the strain of samples to 100, 300, and 500% and back to 0% under the speed of 100 mm min^{-1}. For each maximum strain, the sample was subjected to five cycles of extension. For self-healing testing, the tensile specimens were horizontally cut into halves, then overlapped at the fracture section with an area of 3.18 × 2.00 mm and kept at 140 °C for 30 min under the pressure of 12 MPa and relaxed at room temperature for 24 h before testing. The self-healing efficiency was evaluated by comparing the recovery percentage of the tensile strength and the elongation at break of the healed samples compared to the original samples. Contact angle measurements were detailed in the ESI.† Impedance spectroscopy was carried out using Princeton Applied Research Parastat MC with a PMC-2000 card and a two-point probe between 100 and 10^6 Hz.

2.4 Triboelectric testing

In addition to harvesting energy by the changes in capacitance, there is growing interest in harvesting and sensing via triboelectric effects[16] where charges are produced by contact-separation events. The triboelectric behaviour of the elastomer samples was tested by evaluating the impact force on the material and the resulting triboelectric output voltage generated by each sample. The setup consists of a shaker that is set in a horizontal position, with an electrically insulating wooden plate attached to it that is covered with copper tape (electrode 1) to collect the triboelectric charge, as shown in Fig. 1. In front of the shaker a wooden plate is firmly fixed on a vice with a load cell attached to measure to contact load; the load cell is placed in a standing (vertical) position and carries an insulating wooden plate to which the dielectric elastomer is attached to. Each dielectric elastomer text sample was cut into 50 mm × 50 mm squares and then their backs were covered with conductive carbon to act as an electrode (electrode 2). This type of triboelectric system is called single electrode contact-separation mode, which consists of a single dielectric material (in this case the elastomer) with an electrode attached to its back in contact separation motion with another electrode (in this case copper). This setup was chosen over the dielectric-on-dielectric mode to prevent the effect of other dielectric materials on the triboelectric output.

The load cell output signal was then amplified using the HX711 amplifier and then the amplified signal was converted to load in grams (g) by Arduino Uno. An oscilloscope was used
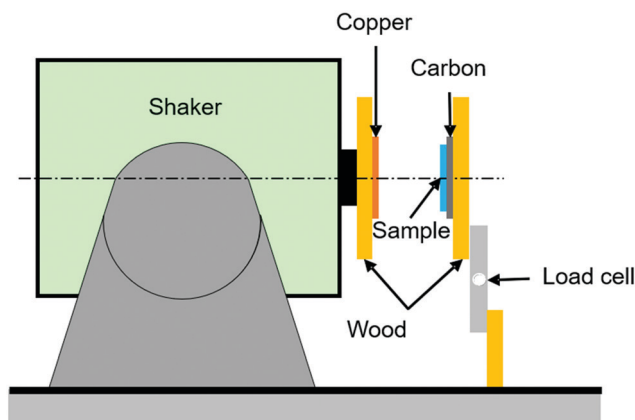

Fig. 1 Schematic of test setup to evaluate triboelectric properties.

to measure the generated voltage, where the copper electrode on the shaker wooden plate was connected to the negative side of the oscilloscope probe and the positive side was connected to the conductive carbon attached to the elastomer sample. The output voltage from the oscilloscope was then plotted side to side with the load from the load cell as shown in Fig. S1 (ESI†). By varying the shaker amplitude, the impact of the copper-covered wooden plate on the sample was varied, as indicated from the varying load on the load cell, which led to different output voltage. The data was collected, and the output voltage was plotted against the load, where the output voltage used in the plots are the peak–peak value.

2.5 Dual-mode cone-shape dielectric elastomer device: principle and set-up

The electro-mechanical properties of the BIIR ionomers can be exploited to convert electrical energy to mechanical energy, and vice versa. With compliant electrodes applied on both faces of a thin film, the sandwiched structure forms a typical Dielectric Elastomer (DE) device that acts as a soft variable capacitor. The capacitance of a DE structure, C_{DE}, can be expressed as

$$C_{DE} = \varepsilon_r \varepsilon_0 \frac{A}{d} \qquad (1)$$

where ε_r is the relative permittivity of the dielectric elastomer, ε_0 is the permittivity of free space, A is the area of the electrode region and d is the thickness of the dielectric elastomer in the electrode region. During mechanical loading (i.e. compression in thickness direction, or extension in planar directions), a deformed dielectric elastomer structure has an enlarged electrode region and a reduced thickness, resulting in an increase in the capacitance. When subjected to loading/unloading cycles, the capacitance change of the dielectric elastomer structure with strain can be used to harvest the mechanical energy and generate electrical energy, by drawing additional electrical charges from the power source and boost them to higher voltages. Conversely, when a high driving voltage (kV) is applied on the electrode region, the induced electrostatic force causes the dielectric elastomer structure to contract in the direction of thickness and expand in plane. The dielectric
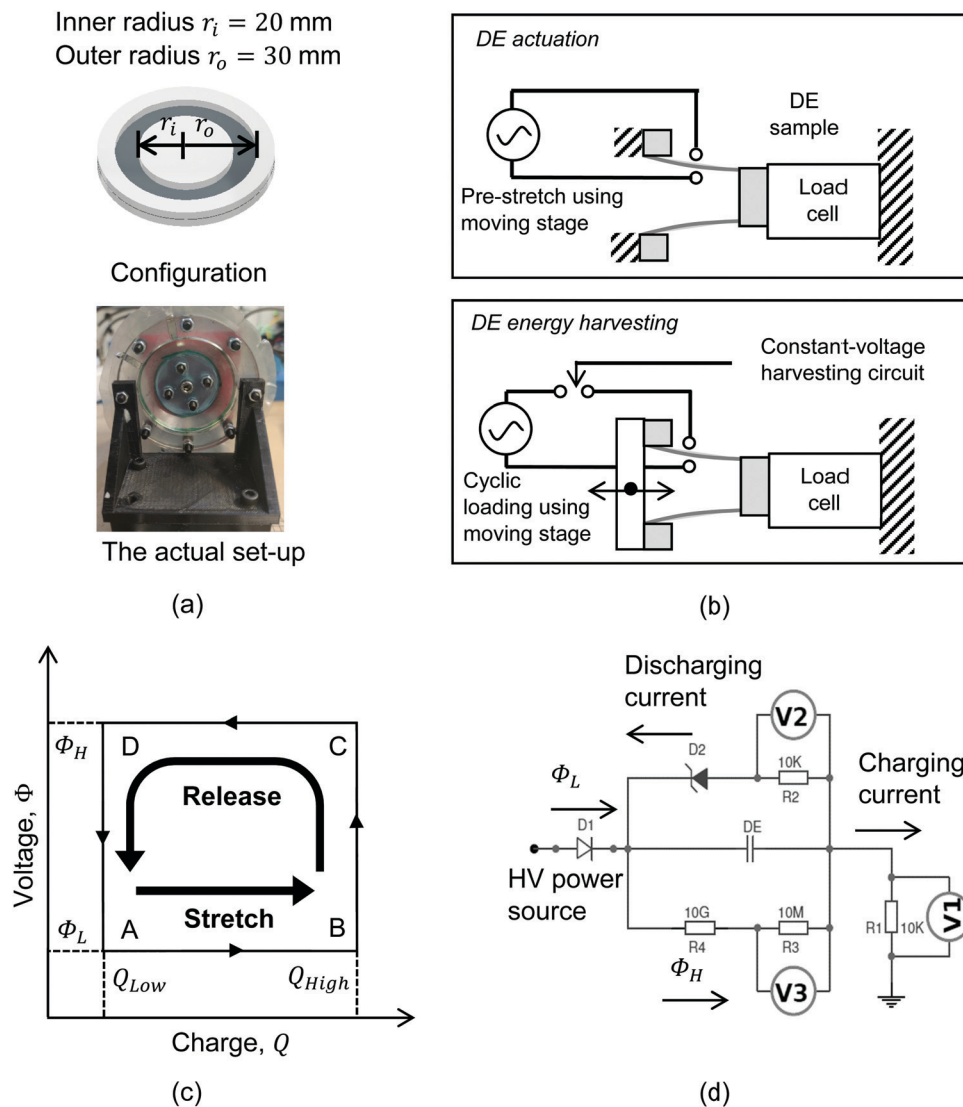
Fig. 2 (a) Configuration of the cone-shaped dielectric elastomer device; (b) schematic of dual-mode operation: actuator mode and energy generator mode; (c) energy harvesting at constant-voltage. The operating principle. From state A to state B: the DE generator draws electrical charges under loading; from state B to state C, D, A: when released, the drawn electrical charges are firstly boosted to have high voltage, then discharged from the DE generator at the constant harvesting voltage until fully depleted as the structure returns to the undeformed shape; (d) the circuit diagram where the meter V1 measures the charging current, V2 measures the discharging current and V3 measures the voltage across the dielectric elastomer generator.

elastomer structure can therefore be used as a soft actuator under electrical stimulations.

To demonstrate the potential modes of operation, the BIIR ionomers were fabricated into a dual-mode cone-shape dielectric elastomer structure, as shown in Fig. 2(a) and (b), to operate in either actuator mode or energy generator mode. A thin elastomer film (~ 350 μm in thickness) was clamped with two sets of rigid frames, namely the inner and outer ring frames. Electrodes (carbon grease from MG Chemicals™) were applied on the elastomer film to form a circular electrode region, with an inner radius $r_i = 20$ mm and an outer radius $r_o = 30$ mm. The dielectric elastomer structure was then mounted on a linear stage that was driven by a stepper motor to stretch the cone-shape device in the direction of thickness. The inner ring frame was stationary and

fixed on a sensor that collects force measurements, while the outer ring frame was mounted on the moving stage, with conductive foils wrapped on the edge for connecting the dielectric elastomer structure to electronic circuits.

In actuator mode, the dielectric elastomer structure is wired directly to the high voltage (HV) power supply and pre-stretched using the moving stage to generate forces under a range of drive voltages. The resulting net forces with and without activation are then calculated to be the force output of the cone-shape actuator. In this work, the BIIR ionomers were pre-stretched with a stroke $l = 20$ mm (i.e. $\Delta A \approx 120\%$), and actuated with a driving voltage, V_A, applied in steps, increasing in magnitude from 0 kV to the point when electrical breakdown occurs. The electric field applied to the electrode region, E_A, is

calculated as

$$E_A = \frac{V_A}{h}(1 + \Delta A) \qquad (2)$$

where h is the thickness of the stretched DE film and ΔA is the areal change in the electrode region that can be estimated as:

$$\Delta A = \frac{(\pi r_o + \pi r_i)\sqrt{(r_o - r_i)^2 + l^2}}{(r_o{}^2 - r_i{}^2)\pi} - 1 \qquad (3)$$

with l being the stroke of the moving stage in relative to the plane of the undeformed DE structure. Note that ΔA in eqn (3) only serves as an estimation of the overall areal strain of the electrode region. The actual deformation of a cone-shape dielectric elastomer structure is inhomogeneous across the electrode region and calculation of exact areal strains requires a sophisticated material model.[17] The actual deformation of the electrode region is larger towards the inner boundary and lower towards the outer boundary, and the estimated electric field using eqn (2) and (3) would be lower than the local maxima and a conservative estimate of the breakdown strength.

In energy generator mode, the cone-shape dielectric elastomer device is wired to an energy harvesting circuit that is powered by a constant driving voltage, and stretched cyclically using the moving stage to convert mechanical energy to electrical energy. For each loading cycle, the dielectric elastomer structure is firstly stretched to have an increased capacitance and draw additional electrical charges from a power source; secondly, the stretched dielectric elastomer is then released, resulting a decrease in the capacitance which leads to a higher voltage for the same level of charge (since $Q = CV$); finally, the dielectric elastomer structure restores the undeformed state and the boosted electrical charges are discharged to the monitoring circuit to undertake measurements. Fig. 2(c) and (d) shows the constant-voltage circuit for energy harvesting. The voltage input is 1.5 kV (i.e. Φ_L = 1.5 kV), where diode D1 blocks the discharged current flow from the dielectric elastomer structure to the power source; D2 is an assembly of Zener diodes in series to establish a constant harvesting voltage of 2 kV (i.e. Φ_H = 2 kV). During mechanical loading, the elastomer is stretched and released at a constant speed of 10 mm s^{-1}, with no pause in between to minimize the effect of stress relaxation on the energy harvesting cycle. The stroke for each test started from l = 10 mm and was increased with an interval of 10 mm to the point until electrical breakdown occurs. At each stroke, the loading cycle was repeated 5 times and the energy harvesting performance was evaluated using the last cycle, to minimize the material stiffening effect on energy harvesting processes.

There are two common ways to drive the energy harvesting circuit, namely the constant-charge method and the constant-voltage method.[18,19] The constant-charge circuit has significantly better performance than the constant-voltage circuit for harvesting energy at higher voltages ($>$2 kV), however, it also requires specialized capacitors, diodes, and switches for operation. This work uses the constant-voltage circuit to perform energy harvesting at lower voltages (2 kV), since the set-up uses

standardised electronic components and offers similar performance. The authors also believe that, while performing energy harvesting at higher voltages with specialized and expensive electronic components can be more efficient, it contradicts the intention of employing dielectric elastomer structures in low-cost applications.

To evaluate the energy harvesting performance, the mechanical energy input, W_M, is calculated as

$$W_M = \int F(t)\mathrm{d}l(t) \qquad (4)$$

where, $F(t)$ is the measured force and $l(t)$ is the displacement of the moving stage. The converted electrical energy, W_E, is calculated as

$$W_E = \Delta Q(\Phi_H - \Phi_L) \qquad (5)$$

with ΔQ being the additional electrical charges that the dielectric elastomer structure draws from the power source due to the change in capacitance. The efficiency of the device that converts mechanical energy to electrical energy can be expressed

$$\eta = \frac{W_E}{W_M} \times 100\% \qquad (6)$$

3. Results and discussion

3.1 Characterisation of BIIR ionomers

A commercial BIIR elastomer has an *exo*-methylene conformation predominantly with minor *endo*-bromomethyl isomers and trace number of other isomers. The BIIR becomes thermally unstable and is subject to the rearrangement of its conformation to more reactive *endo*-bromomethyl isomer at elevated temperature above 85 °C,[5,20] as shown in Fig. 3(a). When bromide ions leave, the process produces a secondary radical on the BIIR backbone (k_2), which rapidly reverses to reform the conventional BIIR (k_{-2}). However, a small number of the radicals generated through this process will initiates propagating radicals/induce coupling reactions between vinyl monomers and BIIR. In addition, BIIR shows high susceptibility to nucleophile substitution, which accelerates the rearrangement and the products are dominated with *endo*-BIIR derivatives pendant with nucleophilic cations.[1,10] Utilising these properties, four types of alkyl imidazoles (EIm, DMIm, HEIm and VIm) with different side groups were selected to compound with BIIR, respectively, and conduct nucleophile substitution reactions at elevated temperatures to form ionically modified BIIR or BIIR ionomers (denoted as BEIm, BDMIm, BHEIm and BVIm). Pyridine (PD) and triphenylphosphine (PPh$_3$) were selected to investigate the effects of different size and properties of nucleophiles, to optimise both the mechanical and dielectric properties of the BIIR ionomers. The substitution reactions were conducted using solid-state compounding and curing process, as illustrated in Fig. 3(b).

The nucleophile substitution reaction proceeds during the compression-moulding process at 140 °C, as monitored by a moving die rheometer; and the relationship between torque
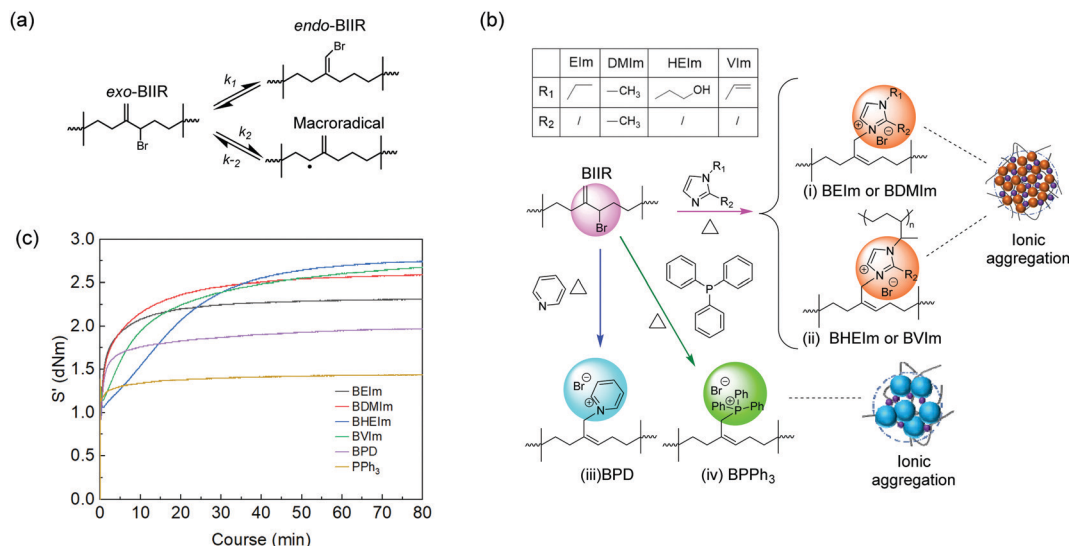
Fig. 3 (a) Schematic of main isomers and intermediates of BIIR rubber during heating; (b) schematic of synthesis of ionic modified BIIR using (i) alkyl imidazoles; (ii) 1-vinyl imidazole, structures shown in the inset table; (iii) pyridine; and (iv) triphenylphosphine; (c) monitoring the ionic clusters formation in different BIIR ionomers using a moving die rheometer.

and moulding time of the BIIR ionomers are shown in Fig. 3(c). The increasing torque with time reveals the progressive formation of ionic aggregates which are composed of bromide anions and pendant imidazolyl, pyridinyl or phosphine cations. The rapid increase of torque at the initial stage was observed for all ionomers, where BEIm showed a high reactivity within the first 4.5 min, and the torque reached a relatively stable

value of ∼2.25 dNm within 20 min. The stabilisation of the torque indicates that the ionic cluster network is formed with a dynamic equilibrium between the association and disassociation of 1-ethyl imidazolyl/bromide ionic interaction. The torque of BDMIm surpasses BEIm after 5 min and reaches 2.45 dNm after 30 min. The slightly higher torque may be due to the more compact ionic interactions as a result of the shorter carbon
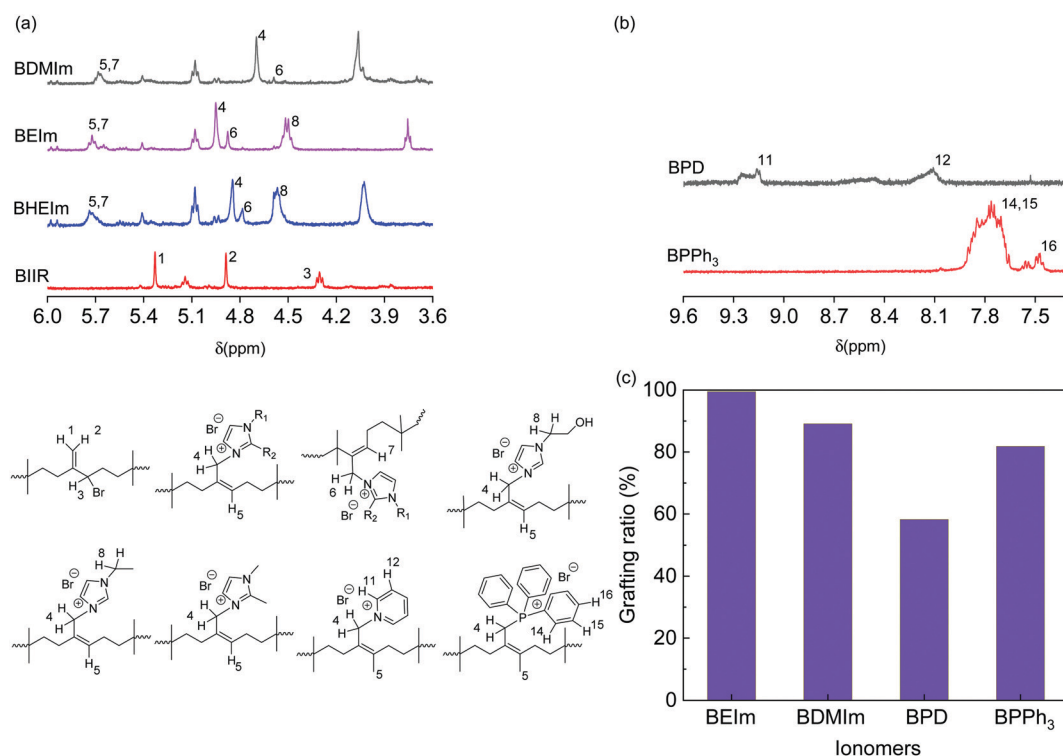

Fig. 4 ^{1}H NMR spectra of (a) pure BIIR, BEIm, BDMIm and BHEIm (dissolved part), and (b) heterocyclic region of BPD and BPPh$_3$ in CDCl$_3$, and (c) grafting ratio of BEIm, BDMIm, BPD and BPPh$_3$ to BIIR.

substituent on the heterocyclic aromatic ring of DMIm.[13] Despite its largest final torque, the curing process and the formation of ionic clusters in BHEIm is retarded at the initial stage as a result of the limited mobility of the HEIm molecules due to the hydrogen bonding between small imidazole-based alcohol molecules in the elastomer matrix. The structure of BEIm, BDMIm and BHEIm (soluble part) was also verified by ^{1}H NMR as shown in Fig. 4(a). The exo-methylene units of pure BIIR are characterised by signals of H1, H2 and H3, and signals of H1 and H2 diminish during heating because of the isomerisation to *endo*-bromomethyl configuration. The success of imidazole alkylation to *endo*-methyl groups in BIIR molecules, is verified by signals of H4 and H6 in the spectra of BEIm, BDMIm and BHEIm (soluble part). Based on the characteristic signals in olefin region (4.0 to 6.0 ppm), considerable grafting ratio of imidazolium alkylation ($>89.0\%$) of BEIm and BDMIm is calculated, shown in Fig. 4(c), which will be obviously beneficial for the production of ionic interactions.[21]

The heterocyclic ring of BEIm, BHEIm and BDMIm is also confirmed with the FTIR spectra, shown in Fig. S2(a) and (b) (ESI†). Peaks at 3580 to 3250 cm^{-1} and 662 cm^{-1} are assigned to the N–H vibration and the out-of-plane deformation, and peaks at 1286 cm^{-1} and 3132 cm^{-1} correspond to the combination of C–H stretching and out-of-plane bending of C–N and the C–H vibration of the imidazole ring.

In the case of BVIm and BHEIm, apart from the alkyl bromide substitution, the existence of bromide leaving group gives rise to macroradicals that may initiate the free radical oligomerisation of vinyl monomers and the grafting of hydroxyl ethylene group or the addition of vinyl monomer to BIIR backbone at elevated temperature, as shown in Fig. 3(a).[22,23] As a result, a network composed of ionic clusters and covalent crosslinks is formed in BVIm and BHEIm. Apart from peaks demonstrating the imidazolyl ring in the ambient FTIR spectra (Fig. S2(a) and (b), ESI†) for BHEIm and BVIm, the peak at 1650 cm^{-1} assigned to the C=C stretching decreases as the temperature increases up to 140 °C in the temperature-dependent FTIR spectra (Fig. S2(d), ESI†) indicating the cross-linking in BVIm.

Both BPD and BPPh$_3$ reach an approximately stable torque value of 1.32 and 1.72 dNm respectively after 7 min, which are much lower than the imidazole modified BIIR. Although PD and PPh$_3$ should be more compatible with the BIIR matrix compared to alkyl imidazoles due to the less polarity, the formation of ionic aggregates is hindered due to the steric effect, and the loose ionic aggregates formed in the matrix in turn affect the mechanical properties of the BIIR ionomers. The signals H11, H12 and H14, H15 and H16 demonstrate pyridine groups and phenyl groups in BPD and BPPh$_3$ respectively as shown in Fig. 4(b), and the olefin region of BPD and BPPh$_3$ is presented in Fig. S3 (ESI†). The aromatic groups are also confirmed in the FTIR spectra of BPD in Fig. S2(a) (ESI†) and BPPh$_3$ in Fig. S2(c) (ESI†). As a result of the steric hindrance, the grafting ratio of BPD and BPPh$_3$ is 58.2% and 81.8% respectively, less than imidazolium BIIR ionomers.
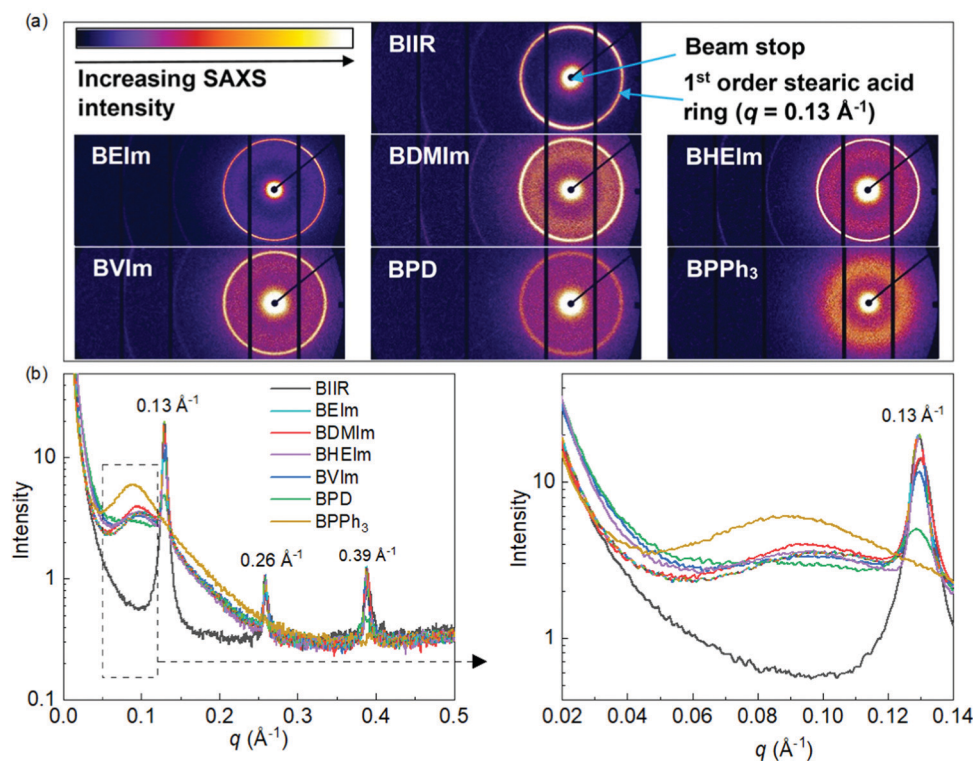

Fig. 5 (a) 2D SAXS data of all samples. The BIIR SAXS pattern shows labelling of the beam stop and the 1st order intense ring of the stearic acid at q = 0.13 Å^{-1}, and (b) 1D SAXS data of BIIR and ionomers and expanded area of the ionic aggregation peaks in ionomer samples (including the stearic acid 1st order peak at 0.13 Å^{-1}).

The development of ionic aggregated macrostructure in the BIIR ionomers can be characterised using Small-Angle X-ray Scattering (SAXS). Fig. 5(a) shows the 2D SAXS patterns of all samples, where the regular sharp rings assigned to stearic acid crystallites are observed, except for the BPPh$_3$ sample. A more diffuse ring (situated near the 1st order stearic acid ring towards the beam stop) is observed in all samples, other than pure BIIR, and this is attributed to the formation of ionic aggregates.

1D SAXS profiles (Fig. 5(b)) were obtained from the 2D SAXS patterns which highlights the ionic aggregates in the ionomers. The 1D SAXS profiles show clearly sharp stearic acid crystal peaks, with regular orders at q = 0.13 Å^{-1}, 0.26 Å^{-1} and 0.39 Å^{-1}, in all samples other than BPPh$_3$. This has been observed by Zhang[24] and Maruyama,[25] and is attributed to the commercial formulation of the BIIR. The absence of stearic acid peaks has been observed before in some ionomer systems, with suggestion that there is a higher solubility of the stearic acid crystallites in the ionic clusters.[24,26] The squared section in Fig. 5(b) was expanded at the right, highlights a second broad peak appearing in all ionomers, except for pure BIIR. The broad peak q = 0.05–0.12 Å^{-1} in the ionomer samples is related to the ionic aggregates with an average correlation length (from the peak position) of $\sim$0.096 Å^{-1}, which is a distance of 65 Å, representing the average distance between the ionic aggregates/clusters. It is worth noting that the BPPh$_3$ ionomer has a more pronounced aggregate peak than the other ionomers and is slightly shifted to a larger correlation length of $\sim$70 Å; this may reflect the size of the PPh$_3$ moiety. Therefore, BPD appears to have the least ionic aggregation, due to the least grafting ratio of PD to BIIR molecules. In summary, the SAXS data has clearly shown that all the ionomers show ionic aggregation to varying degrees when compared to pure BIIR.

The ionic association of the BIIR ionomers was further characterised by DMTA. The storage modulus (E') of BIIR ionomers in the temperature range from −65 to 120 °C were investigated, as shown in Fig. 6(a). In the temperature range from −65 to 0 °C, the storage moduli of all the ionomers decreased with temperature due to the glass-rubbery transition of the polymer chain segments, among which the E' of BPD is the lowest because a lower degree of reinforcement is imposed on the BIIR molecular chains due to fewer ionic interactions between pyridine grafted IIR cations and bromide anions. In the rubbery region, both BDMIm and BVIm show a plateau of E' before further decreasing at 65 °C, while the E' of BHEIm decreases slightly compared to other BIIR ionomers. The storage modulus E' reflects the capacity of elastomers to store energy during deformation.[27] The stronger ionic interactions of BDMIm make it more stable than other BIIR ionomers, while the E' of BPD and BPPh$_3$ decrease continuously with increasing temperature, indicating weaker ionic interactions.

Fig. 6(b) and Table 1 show the loss modulus (E'') transition information of the BIIR ionomers. The temperature of the relaxation peak of E'' below 0 °C is regarded as T_g, shown in Table 1. The BDMIm, BHEIm and BVIm show glass-rubber transition peaks (T_g) at approximately −56 °C, while BPD and BPPh$_3$ show slightly lower glass-rubber transition temperatures of T_g = −65.8 and T_g = −60.8 °C, respectively. A second transition is observed for all the ionomers between 50 and 100 °C, indicating the dissociation of the ionic aggregates. The transition temperature (T_{ion}) is related to the structure rearrangement of the ionic clusters and the ionic interactions[28] which gives the ionomer the susceptibility to heal at elevated temperatures. The BHEIm exhibits the highest T_{ion} = 96.4 °C with the smallest E'' peak, which may be caused by the dual effect of hydrogen bonding originated from the pendant –OH groups and the ionic bonds, as discussed in Fig. S2(a) (ESI†).

3.2 Mechanical and self-healing properties

The self-healing performance of BIIR ionomers were investigated by tensile tests, where the stress–strain behaviour of BIIR ionomers before and after treatment of 140 °C for 30 min are compared in Fig. 7, and results are summarised in Table 1. It can be seen that the four alkyl imidazole modified BIIR ionomers exhibit outstanding mechanical properties with tensile strength and elongation at break in excess of 14.5 MPa and 1350%. In particular, BDMIm has the highest tensile strength of 20.13 ± 4.32 MPa, elongation at break of 1684 ± 170% and
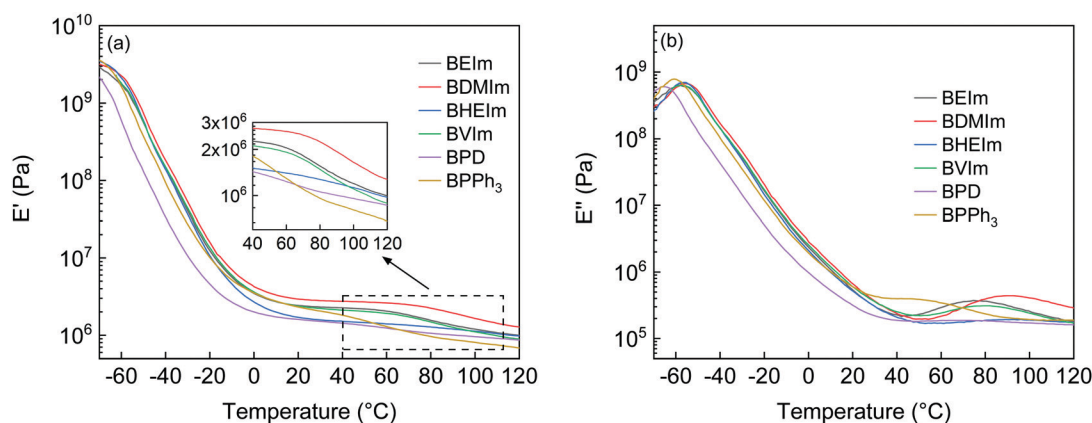

Fig. 6 (a) E' and (b) E'' vs. frequency curve of BIIR ionomers between −65 °C and 120 °C at 10 Hz.

Table 1 Thermal, mechanical, dielectric properties and electrical breakdown (EB) strength of BIIR ionomers

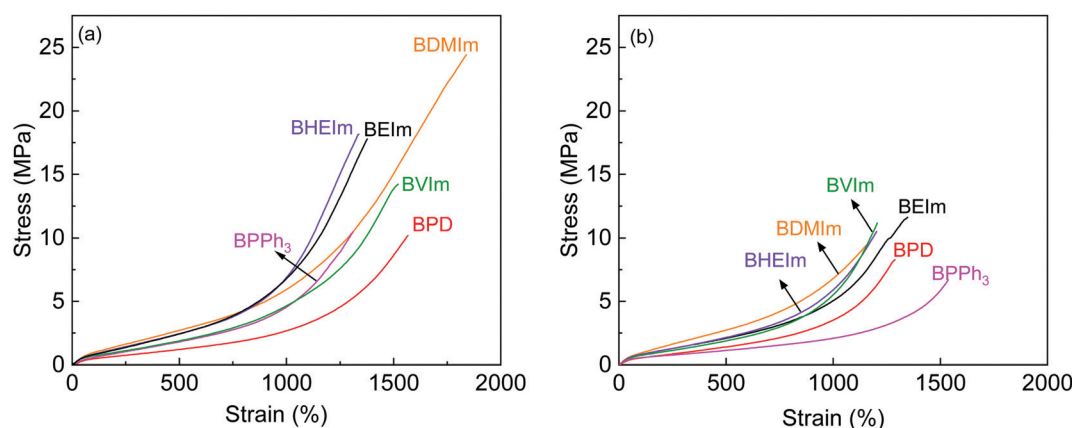| Samples	T_g (°C)	T_{ion} (°C)	Dielectric permittivity at 10^3 Hz	EB field (MV m^{-1})	Tensile strength (MPa)	Elongation at break (%)	Stress at 300% (MPa)	Self-healing efficiency (%) (140 °C, 30 min)	
								Tensile strength	Elongation at break
BEIm	−57.0	74.6	3.10	—	17.01 ± 1.89	1402 ± 69	1.82 ± 0.31	63.7	88.9
BDMIm	−55.8	89.8	2.90	—	20.13 ± 4.32	1684 ± 170	1.85 ± 0.03	49.5	68.3
BHEIm	−56.5	96.4	3.14	29.58	16.89 ± 1.72	1390 ± 53	1.40 ± 0.21	48.0	82.4
BVIm	−56.7	79.1	2.89	26.14	14.66 ± 2.26	1561 ± 186	1.34 ± 0.10	68.8	78.7
BPD	−65.8	71.7	2.84	18.09	11.43 ± 1.26	1616 ± 50	0.94 ± 0.06	72.4	81.4
BPPh$_3$	−60.8	50.4	3.71	35.19	11.46 ± 3.29	1410 ± 212	1.20 ± 0.04	56.0	108.1
Sulfur-cured BIIR	−56.0	—	2.86	—	12.03 ± 1.77	1389 ± 95	0.93 ± 0.02	—	—

stress at 300% strain of 1.85 ± 0.03 MPa among the BIIR ionomers. These properties lead to BDMIm outperforming BVIm and BHEIm which contain ionic crosslinks and potentially covalent crosslinks, and even outperforming sulfur cured BIIR (tensile strength 12.03 ± 1.77 MPa, elongation at break 1389 ± 95%, stress at 300% strain 0.93 ± 0.02 MPa). This is consistent with the curing properties discussed in Fig. 4(B), where the shorter alkyl substitutes provide a denser ionic network. BPD and BPPh$_3$ are much weaker than the imidazole modified BIIR ionomers mainly due to the lower grafting ratio and the loose ionic aggregates formed by the bulky ionic side groups separately. The relatively high elongation at break of BPD could be attributed to the plasticization of excessive PD molecules distributed in the polymer.

Thanks to the dynamic nature of the network, all BIIR ionomers exhibit self-healing behaviour with regard to both tensile strength and elongation at break at elevated temperature which is higher than T_{ion}. For BIIR ionomers crosslinked solely by ionic aggregates, BEIm, BDMIm, BPD and BPPh$_3$, BPD achieves the highest healing efficiency by retaining 72.4% of its original tensile strength, because of a high re-assembly degree of ionic aggregates without steric hindrance of substituents on the ring; and BPPh$_3$ shows the highest efficiency of 108.1% in terms of elongation at break, which can be attributed to a higher dis-entanglement of molecule chains due to the weak restrict on the molecule mobility from the grafted PPh$_3^+$–Br$^-$

interactions. The healing efficiency of BEIm in both tensile strength and elongation at break is higher than that of BDMIm, which is regarded as the consequence of the higher susceptibility to rearrangement of less dense ionic interactions in the reconnected region due to the longer substitute on the imidazole ring. BIIR ionomers containing hybrid networks also exhibit self-healing behaviour thanks to both the rearrangement of ionic clusters and the production of new hybrid crosslinking at 140 °C, and BVIm maintains a healing efficiency even higher than that of BEIm in tensile strength. Overall, BEIm shows the best balance of self-healing and mechanical properties among all the BIIR ionomers as discussed above.

The strength and stability of the ionic interactions in different BIIR ionomers are further investigated by cyclic tensile testing. Fig. 8 compares the cyclic testing of BDMIm and BPPh$_3$ after cycle 1 and cycle 5 at extension of 100, 300 and 500%, respectively. The testing results of other BIIR ionomers are shown in Fig. S4 (ESI†). The maximum strength at given strains reflects the ionic interaction strength. BDMIm exhibits the highest strength among all other ionomers, while the BPPh$_3$ shows the lowest strength, which is consistent with the tensile property discussed in Fig. 8. For each cycle, the hysteresis of alkyl imidazole modified BIIR are more prominent than those of BPD and BPPh$_3$ at the given extension deformation (Fig. 7 and Fig. S4(a)–(d), ESI†), indicating that stronger ionic interactions in imidazolium BIIR ionomers consume more

Fig. 7 Stress−strain curves of BIIR ionomers (a) before and (b) after self-healing @140 °C for 30 min.
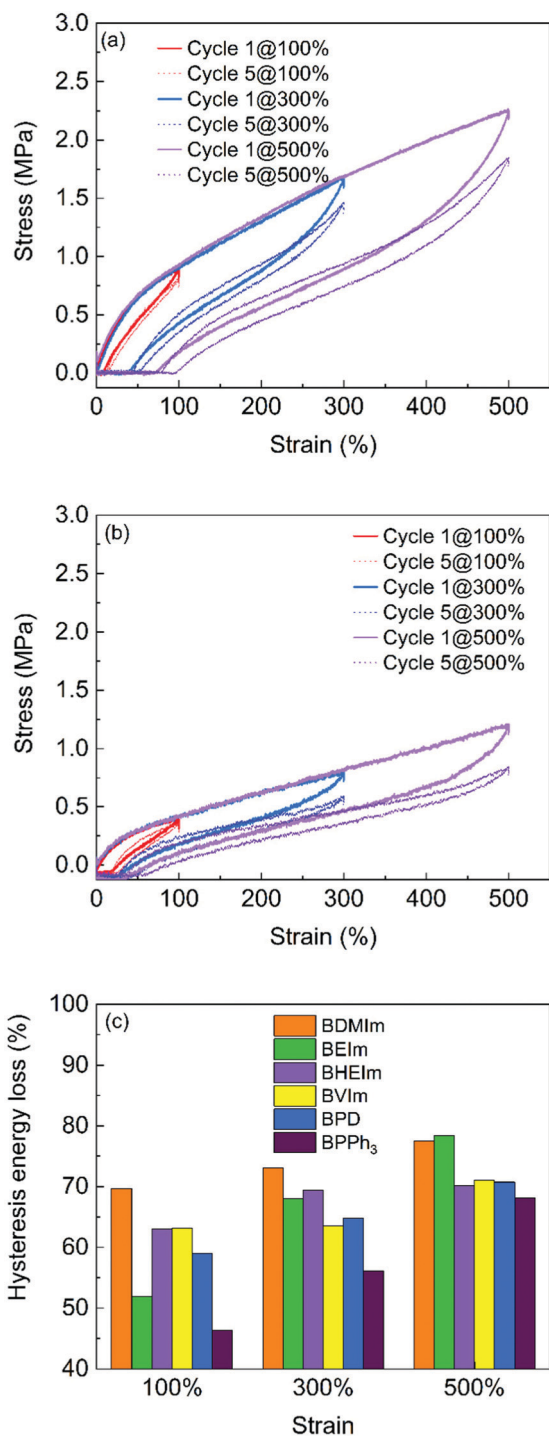
Fig. 8 Cyclic tensile testing of (a) BDMIm; (b) BPPh$_3$ with the maximum strain at 100%, 300% and 500% and (c) hysteresis energy loss of the BIIR ionomers after 5 cycles of extension.

Fig. 9 The triboelectric performance of BIIR ionomers.

energy for their dissociation. The hysteresis losses after five cycles of extension of all the BIIR ionomers exceed 50%, and further increase with an increase of the maximum strain.

The output of triboelectric performance is shown in Fig. 9. Among the four samples, sulfur-cured BIIR shows the highest voltage output ranged from 12 V to 20 V with an impact load that varied between 150 g to 350 g. The three ionic-modified

BIIR samples showed output voltage at a smaller scale in the same impact load range. BVIm and BDIm had higher slope thus the output voltage varied with respect to the load with a range of 2.5 V to 4 V. On the other hand, BHEIm gave out a fixed voltage varying close to the 1.5 V.

The impact on materials properties and composition has been examined by a number of researchers.[29–31] The triboelectric effect has been overviewed by Pan et al.,[29] where the triboelectric series provides details on the level of charging when two materials are brought into contact through rubbing, pressing, or friction. It was thought that polymers which have a strong tendency to charge positively and have a higher relative permittivity, are highly polar and are hydrophilic; functionalization of surfaces with highly polarized functional groups has also been considered.[30] However, the sulfur-cured BIIR has a slightly lower relative permittivity ($\varepsilon_r \sim 2.86$) compared to BVIm ($\varepsilon_r \sim 2.89$), BDMIm ($\varepsilon_r \sim 2.90$), and BHEIm ($\varepsilon_r \sim 3.14$); see Table 1. In addition, the contact angle and surface energy are not significantly different for the materials examined, see Table S2 (ESI†). While temperature and humidity can also impact the triboelectric response,[29,30] all testing was undertaken at the same condition. One difference is that the sulfur-cured BIIR has a low stiffness with a relatively low stress at 300% strain of 0.93 MPa (see Table 1), as compared to BVIm (1.34 MPa), BDMIm (1.85 MPa), and BHEIm (1.4 MPa). The lower stiffness of sulfur-cured could lead to greater degree of surface contact as it is deformed during contact-separation events. The impact of material stiffness was also overview by Li et al.[31] who described material transfer mechanisms during contact events and its correlation with the elastic modulus and cohesive energy of the material, where the lower stiffness promoted the transfer of charged segments and will help enhance the voltage generated in Fig. 9.

3.3 Dielectric BIIR ionomers for energy harvesting and actuation

The effect of the introduction of nucleophiles on dielectric property of BIIR ionomer is investigated, as shown in Fig. 10(a)
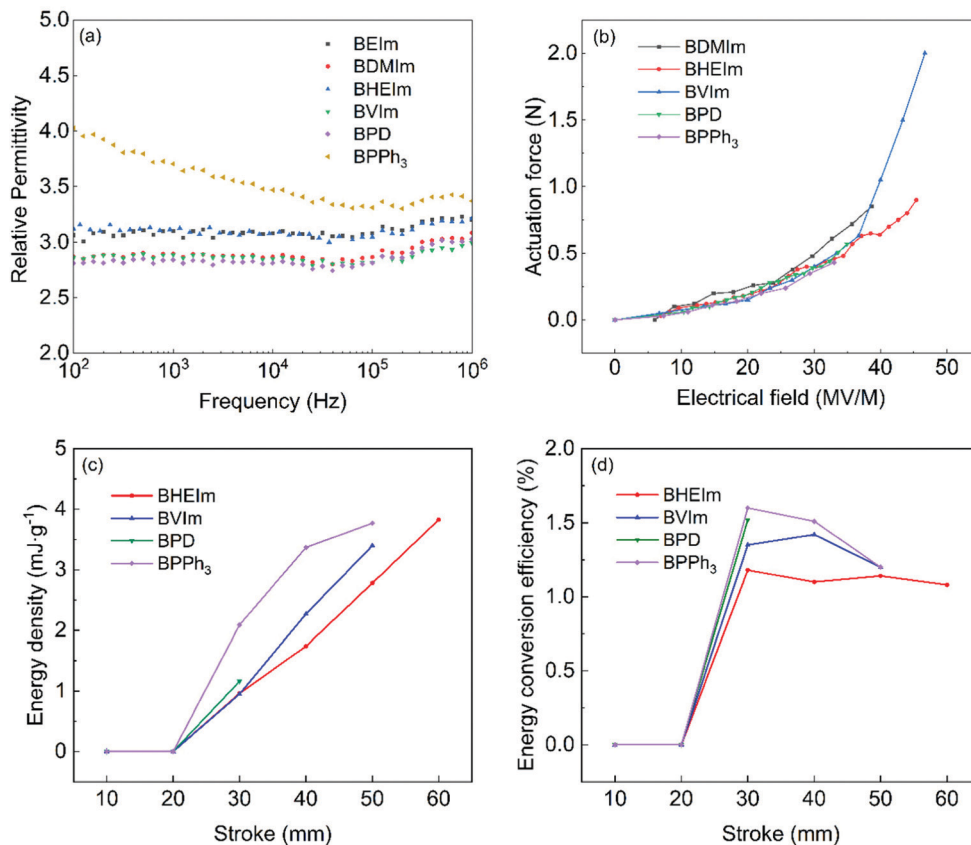
Fig. 10 (a) Relative permittivity of BIIR ionomers, (b) force outputs, (c) energy density and (d) energy conversion efficiency of conical BIIR ionomers based dielectric elastomer actuator.

and Fig. S5 (ESI†). The relative permittivity of imidazolium and pyridine BIIR ionomers remains stable between 10^2–10^6 Hz, with a value of ε_r = 2.80–3.10 at 10^3 Hz, and the enhancement is small compared to sulfur cured BIIR ($\varepsilon_r \sim$ 2.86 at 10^3 Hz). For all BIIR ionomers, the cations are covalently anchored to the molecule backbones (see Fig. 3(b)), and the anions are immobilized by the ionic clusters to some degree, as a result, the relative permittivity should be related to the dissociation of ionic clusters under the electric field.[32] As previously mentioned, more compact ionic clusters are formed in the imidazolium BIIR ionomers, leading to an only slightly increased relative permittivity of imidazolium BIIR ionomers, and BPD also show limited relative permittivity due to its low polarity which has an effect on the dielectric property of the polymer.[33] BPPh$_3$ shows a higher relative permittivity ($\varepsilon_r \sim$ 3.71 at 10^3 Hz) which is dependent on the frequency. This is associated with the higher conductivity of BPPh$_3$, see Fig. S4(a) (ESI†).

Fig. 10(b) shows the BIIR ionomers have similar performances in actuation at electrical fields up to 35 MV m^{-1}, with the BVIm generating the highest force of 2 N at a maximum electrical field of 47 MV m^{-1}. The BDMIm, BHEIm, BPD and BPPh$_3$, generate the maximum forces of 0.85, 0.9, 0.57 and 0.43 N, at the electrical fields of 39 and 45, 35 and 33 MV m^{-1}, respectively. In comparison, the VHB-4910 polyacrylate, the commonly used DE, generates a maximum force output of 1.7 N in a similar conical configuration for DE actuations.[17]

The difference may appear to be small, but the polyacrylate-based actuator has an electrode region with the inner radius of 15 mm and the outer radius of 45 mm and a total area of the electrode region of $A = 5.7 \times 10^3$ mm^2, over 3.5 times larger than that of $A = 1.6 \times 10^3$ mm^2 in the BVIm-based actuator. In terms of the maximum force output per area, the BVIm is over three times higher than the VHB-4910 polyacrylate.

Fig. 10(c) shows that BVIm, BHEIm and BPPh$_3$ have similar maximum energy densities of 3.40, 3.83, 3.77 mJ g^{-1} respectively. The BPD has the lowest energy density of 1.16 mJ g^{-1} due to the low breakdown strength of 18 MV m^{-1} in energy harvesting tests. The energy harvesting cycles at low strokes of 10 mm and 20 mm are heavily affected by relaxation, resulting low electrical energy output. Compared with the actuation results, the energy generators fail at a lower electrical field due to defects and stress concentration at larger deformation (stroke > 20 mm).

Fig. 10(d) shows that BHEIm, BVIm, BPD and BPPh$_3$ have similar peak energy conversion efficiencies of 1.4%, 1.2%, 1.5% and 1.6% at the stroke of 30, 40, 30 and 30 mm respectively. After reaching the peak values, the energy conversion efficiencies of BHEIm, BVIm and the BPPh$_3$ decrease as the strokes increases further due to factors such as relaxation, and deterioration in electrode coverage. In overall, the energy harvesting performance of BHEIm, BVIm and BPPh$_3$ are comparable to a polyacrylate without pre-stretch (i.e. VHB 4905) under similar

configurations in energy harvesting, which has an energy conversion efficiency below 2% and an energy density below 2 mJ g^{-1}.[34]

The actual energy conversion of a conical DE generator is found to be strongly affected by two factors: the inhomogeneous deformation and the relaxation effect. The inhomogeneous deformation causes pre-mature electrical breakdown, and the relaxation effect leads to slowness of the stretched DE generator in restoring its un-deformed shape, which can be significantly compared with a typical cycle time in energy harvesting experiments. Continuing loading cycles without restoring the un-deformed shape would result a decrease in the capacitive change and therefore lower the generated electrical energy. Moreover, the conventional method of calculating energy conversion efficiency of a DE generator also takes account the energy dissipation of the DE due to viscoelasticity during the energy harvesting process. Since a DE generator also behaves like a damper, the energy dissipation process and the energy harvesting process, although not dependent of each other, are coupled and occur simultaneously. As with the dielectric constant (relative permittivity) and breakdown strength of DEs, the viscoelasticity of DEs therefore also affects how much electrical energy is generated from a given amount of mechanical energy. A strong viscoelastic behaviour can hinder the energy conversion efficiency in a DE generator even though its dielectric constant and breakdown strength are high; on the other hand, reducing viscoelastic behaviour is a valid option to optimize DEs for energy harvesting processes.

In contrast, there are also factors that should be neglected in evaluating the energy harvesting performances of DE generators. Through experiment studies, it is found that loss of charges always occurs in energy harvesting due to energy dissipation during the process and is observed as a decrease in electrical charges in charging/discharging cycles. The loss of charges is a result of two sources: through the energy harvesting circuit and through the DE structure. The former occurs when the circuit is in operation and can cause a typical loss of charge in the magnitude 10 μC.[19] It is solely associated with the circuit set-up for monitoring changes in voltage and current. Such a loss of charges is only negligible when the test is conducted on a larger DE energy generator with the measured capacitive change being relatively large, in 100 μC or higher. The latter is due to defects that arise from the fabrication process or conductivity.[35] Defects or conductivity in the materials make a DE structure behaves like a resistor and a capacitor connecting in parallel, where the resistance of the resistor is proportional to deformation of the DE structure. For example, it was observed that current leakage occurs in the magnitude 1 μA under a driving voltage of 1.5 kV and increases with the driving voltage. In the case of a high loss of charges and current leakage, the level of energy dissipation can occur at a higher rate than the energy generation, leading to a loss of all electrical charges during the discharging process. As a result, neither discharging current nor increase in voltage output would be observed.

As the fabrication process for synthesizing DEs improves, the defects and the associated current leakage would be minimized, as in the commercially available polyacrylate (e.g. VHB 4910 and VHB 4905). The method of excluding current leakage is described in the previous work.[35] To exclude the energy dissipation of the harvesting circuit, it is assumed that no charges are lost during the process and the electrical energy is generated at the constant harvesting voltage, which is configured to be close to the input voltage (e.g. Φ_H = 2 kV and Φ_L = 1.5 kV).

4. Conclusions

BIIR ionomers were prepared via nucleophile substitution of three types of nucleophile reagents using solid-state rubber compounding and curing process. The nucleophile substitution resulted ionic clusters formed of grafted nucleophile cations and bromide anions in the elastomer, the presence and size of the ionic clusters were characterised by SAXS. The ionic transition temperature ranges between 50 and 100 °C that is related to the rearrangement of the ionic aggregates are determined by DMTA.

The 1-ethyl imidazole (EIm) modified BIIR exhibited the highest mechanical and self-healing properties. The ionically modified BIIR exhibited similar actuation performance at electrical fields up to 35 MV m^{-1}, in which the BVIm generated the highest force of 2 N at a maximum electrical field of 47 MV m^{-1}, and the maximum force output per area of BVIm-based actuator is 3 times higher than commercial polyacrylate VHB-4910. The maximum energy density of BHEIm, BVIm and BPPh$_3$ was between 3.40 and 3.83 mJ g^{-1} with the energy conversion efficiency at around 1.2 to 1.6%. Overall, BVIm and BHEIm are comparable to VHB-4905 without pre-stretching in energy harvesting, and also have high mechanical properties and self-healing performance simultaneously.

Conflicts of interest

The authors declare that they have no competing financial interests or personal relationships that could have appeared to influence the work reported in this paper.

Acknowledgements

References

1 J. S. Parent, A. M. J. Porter, M. R. Kleczek and R. A. Whitney, Imidazolium bromide derivatives of poly(isobutylene-co-isoprene): A new class of elastomeric ionomers, *Polymer*, 2011, **52**(24), 5410–5418, DOI: **10.1016/j.polymer.2011.10.021**.

2 S. Stein, A. Mordvinkin, B. Voit, H. Komber, K. Saalwächter and F. Böhme, Self-healing and reprocessable bromo

butylrubber based on combined ionic cluster formation and hydrogen bonding, *Polym. Chem.*, 2020, **11**(6), 1188–1197, DOI: **10.1039/c9py01630a**.

3 S. A. Guillén-Castellanos, J. S. Parent and R. A. Whitney, Synthesis and characterization of ether derivatives of brominated poly(isobutylene-*co*-isoprene), *J. Polym. Sci., Part A: Polym. Chem.*, 2006, **44**(2), 983–992, DOI: **10.1002/pola.21221**.

4 M. R. Kleczek, R. A. Whitney, A. J. Daugulis and J. S. Parent, Synthesis and characterization of thermoset imidazolium bromide ionomers, *React. Funct. Polym.*, 2016, **106**, 69–75, DOI: **10.1016/j.reactfunctpolym.2016.07.019**.

5 J. R. McNeish, J. S. Parent and R. A. Whitney, Halogenated poly(isobutylene-*co*-isoprene): influence of halogen leaving-group and polymer microstructure on chemical reactivity, *Can. J. Chem.*, 2013, **91**(6), 420–427, DOI: **10.1139/cjc-2013-0068**.

6 A. Ozvald, J. Scott Parent and R. A. Whitney, Hybrid ionic/covalent polymer networks derived from functional imidazolium ionomers, *J. Polym. Sci., Part A: Polym. Chem.*, 2013, **51**(11), 2438–2444, DOI: **10.1002/pola.26629**.

7 A. A. Ozvald, M. R. Klezcek, A. C. Rodrigo and J. S. Parent, Isobutylene-Rich Imidazolium Ionomers: Influence of Ion-Pair Distribution and Counter-Anion Structure, *Rubber Chem. Technol.*, 2018, **91**(2), 303–319, DOI: **10.5254/rct.18.83700**.

8 J. S. Parent, A. Liskova and R. Resendes, Isobutylene-based ionomer composites: siliceous filler reinforcement, *Polymer*, 2004, **45**(24), 8091–8096, DOI: **10.1016/j.polymer.2004.09.051**.

9 J. S. Parent, S. M. Malmberg and R. A. Whitney, Autocatalytic chemistry for the solvent-free synthesis of isobutylene-rich ionomers, *Green Chem.*, 2011, **13**(10), 2818–2824, DOI: **10.1039/c1gc15638a**.

10 J. S. Parent, A. Penciu, S. A. Guillen-Castellanos, A. Lišková and R. A. Whitney, Synthesis and Characterization of Isobutylene-Based Ammonium and Phosphonium Bromide Ionomers, *Macromolecules*, 2004, **37**, 7477–7483.

11 S. Xiao, J. S. Parent, R. A. Whitney and L. K. Knight, Synthesis and characterization of poly(isobutylene-*co*-isoprene)-derived macro-monomers, *J. Polym. Sci., Part A: Polym. Chem.*, 2010, **48**(21), 4691–4696, DOI: **10.1002/pola.24256**.

12 V. D. Deepak, I. Mahmud and M. Gauthier, Synthesis of carboxylated derivatives of poly(isobutylene-*co*-isoprene) by azide–alkyne "click" chemistry, *Polym. J.*, 2019, **51**(3), 327–335, DOI: **10.1038/s41428-018-0130-y**.

13 M. Suckow, A. Mordvinkin, M. Roy, N. K. Singha, G. Heinrich, B. Voit, K. Saalwächter and F. Böhme, Tuning the properties and self-healing behavior of ionically modified poly(isobutylene-*co*-isoprene) rubber, *Macromolecules*, 2017, **51**(2), 468–479, DOI: **10.1021/acs.macromol.7b02287**.

14 A. Das, A. Sallat, F. Bohme, M. Suckow, D. Basu, S. Wiessner, K. W. Stockelhuber, B. Voit and G. Heinrich, Ionic modification turns commercial rubber into a self-healing material, *ACS Appl. Mater. Interfaces*, 2015, **7**(37), 20623–20630, DOI: **10.1021/acsami.5b05041**.

15 L. Zhang, H. Wang, Y. Zhu, H. Xiong, Q. Wu, S. Gu, X. Liu, G. Huang and J. Wu, Electron-Donating Effect Enabled Simultaneous Improvement on the Mechanical and Self-Healing Properties of Bromobutyl Rubber Ionomers, *ACS Appl. Mater. Interfaces*, 2020, **12**(47), 53239–53246, DOI: **10.1021/acsami.0c14901**.

16 T. S. Natarajan, S. Finger, J. Lacayo-Pineda, E. S. Bhagavatheswaran, S. S. Banerjee, G. Heinrich and A. Das, Robust Triboelectric Generators by All-In-One Commercial Rubbers, *ACS Appl. Electron. Mater.*, 2020, **2**(12), 4054–4064, DOI: **10.1021/acsaelm.0c00846**.

17 H. M. Wang, J. Y. Zhu and K. B. Ye, Simulation, experimental evaluation and performance improvement of a cone dielectric elastomer actuator, *J. Zhejiang Univ., Sci., A*, 2009, **10**(9), 1296–1304, DOI: **10.1631/jzus.A0820666**.

18 S. Shian, J. Huang, S. Zhu and D. R. Clarke, Optimizing the Electrical Energy Conversion Cycle of Dielectric Elastomer Generators, *Adv. Mater.*, 2014, **26**(38), 6617–6621.

19 J. Huang, S. Shian, Z. Suo and D. R. Clarke, Maximizing the energy density of dielectric elastomer generators using equi-biaxial loading, *Adv. Funct. Mater.*, 2013, **23**(40), 5056–5061, DOI: **10.1002/adfm.201300402**.

20 S. M. Malmberg, J. S. Parent, D. A. Pratt and R. A. Whitney, Isomerization and Elimination Reactions of Brominated Poly(isobutylene-*co*-isoprene), *Macromolecules*, 2010, **43**(20), 8456–8461, DOI: **10.1021/ma1018268**.

21 I. I. Smolentseva, V. I. Mashukov and E. I. Korotkova, Determination of Unsaturation Level, Halogen Content, and Main Forms of Isoprene Units in Halogenated Butyl Rubbers by 1H NMR Spectroscopy, *J. Appl. Spectrosc.*, 2015, **82**(3), 465–469, DOI: **10.1007/s10812-015-0131-y**.

22 K. E. Russell, Free radical graft polymerization and copolymerization at higher temperatures, *Prog. Polym. Sci.*, 2002, **27**(6), 1007–1038, DOI: **10.1016/S0079-6700(02)00007-2**.

23 J. S. Parent, D. J. Thom, G. White, R. A. Whitney and W. Hopkins, Thermal Stability of Brominated Poly(isobutylene-coisoprene), *J. Polym. Sci., Part A: Polym. Chem.*, 2001, **39**, 2019–2026.

24 L. Zhang, H. Wang, Y. Zhu, H. Xiong, Q. Wu, S. Gu, X. Liu, G. Huang and J. Wu, Electron-Donating Effect Enabled Simultaneous Improvement on the Mechanical and Self-Healing Properties of Bromobutyl Rubber Ionomers, *ACS Appl. Mater. Interfaces*, 2020, **12**(47), 53239–53246, DOI: **10.1021/acsami.0c14901**.

25 T. Maruyama, M. Nakajima, S. Ichikawa, Y. Sano, H. Nabetani, S. Furusaki and M. Seki, Small-Angle X-Ray Scattering Analysis of Stearic Acid Modified Lipase, *Biosci., Biotechnol., Biochem.*, 2001, **65**(4), 1003–1006, DOI: **10.1271/bbb.65.1003**.

26 A. Mordvinkin, M. Suckow, F. Böhme, R. H. Colby, C. Creton and K. Saalwächter, Hierarchical Sticker and Sticky Chain Dynamics in Self-Healing Butyl Rubber Ionomers, *Macromolecules*, 2019, **52**(11), 4169–4184, DOI: **10.1021/acs.macromol.9b00159**.

27 A. Dziemidkiewicz, M. Maciejewska and M. Pingot, Thermal analysis of halogenated rubber cured with a new cross-linking system, *J. Therm. Anal. Calorim.*, 2019, **138**(6), 4395–4405, DOI: **10.1007/s10973-019-08881-7**.

28 D. Huang, Y. Ding, H. Jiang, S. Sun, Z. Ma, K. Zhang, L. Pan and Y. Li, Functionalized Elastomeric Ionomers Used as

Effective Toughening Agents for Poly(lactic acid): Enhancement in Interfacial Adhesion and Mechanical Performance, *ACS Sustainable Chem. Eng.*, 2019, **8**(1), 573–585, DOI: **10.1021/acssuschemeng.9b06123**.

29 S. Pan and Z. Zhang, Fundamental theories and basic principles of triboelectric effect: A review, *Friction*, 2019, **7**(1), 2–17, DOI: **10.1007/s40544-018-0217-7**.

30 Y. S. Choi, S. W. Kim and S. Ka' Narayan, Material-Related Strategies for Highly Efficient Triboelectric Energy Generators, *Adv. Energy Mater.*, 2021, **11**, 2003802.

31 J. Li, N. A. Shepelin, P. C. Sherrell and A. V. Ellis, Poly(dimethylsiloxane) for Triboelectricity: From Mechanisms to Practical Strategies, *Chem. Mater.*, 2021, **33**(12), 4304–4327, DOI: **10.1021/acs.chemmater.1c01275**.

32 U. H. Choi, T. L. Price, D. V. Schoonover, R. X. Xie, H. W. Gibson and R. H. Colby, Role of Chain Polarity on Ion and Polymer Dynamics: Molecular Volume-Based Analysis of the Dielectric Constant for Polymerized Norbornene-Based Ionic Liquids, *Macromolecules*, 2020, **53**(23), 10561–10573, DOI: **10.1021/acs.macromol.0c02100**.

33 E. Christopher, R. Zhang, A. M. Wemyssc, C. Bowenb, T. McNallya, Ł. Figiela and C. Wan, Intrinsic tuning of styrene-butadiene-styrene (SBS) based self-healing dielectric elastomer actuators with enhanced electromechanical properties, *ACS Appl. Mater. Interfaces*, 2020, **8**(22), 6167–6173.

34 Y. Jiang, S. Liu, M. Zhong, L. Zhang, N. Ning and M. Tian, Optimizing energy harvesting performance of cone dielectric elastomer generator based on VHB elastomer, *Nano Energy*, 2020, **71**, DOI: **10.1016/j.nanoen.2020.104606**.

35 C. Ellingford, R. Zhang, A. M. Wemyss, Y. Zhang, O. B. Brown, H. Zhou, P. Keogh, C. Bowen and C. Wan, Self-healing dielectric elastomers for damage-Tolerant actuation and energy harvesting, *ACS Appl. Mater. Interfaces*, 2020, **12**(6), 7595–7604, DOI: **10.1021/acsami.9b21957.s**.